INTERNAL REPORT

Space Debris forecasting campaign

T. Pisanu (INAF-OAC), E. Urru (INAF-OAC), G. Muntoni (UniCa-DIEE), L. Schirru (INAF-OAC), F. Gaudiomonte (INAF-OAC), G. Valente (INAF-OAC), G. Serra (INAF-OAC).

REPORT N. 61

RELEASED: 10/01/2017

REVIEWER: Germano Bianchi (INAF-IRA)

OAC Osservatorio Astronomico di Cagliari

PREFACE

TECHNICAL REPORT

Space Debris Forecasting Campaign

SUMMARY

1. INTRODUCTION

The Space Debris monitoring is part of the INAF-OAC research activity in the framework convention ASI/INAF n. 2015-028-R.O, named "Detriti Spaziali – Supporto alle attività IADC e validazione pre-operativa SST". In this framework, the INAF participation concerns about the testing of the SRT operative capacities in the detection of signals scattered by Space Debris, illuminated using RADAR systems in P band.

This report aims to provide a brief overview on space debris problem and, principally, to organize a forecasting campaign, knowing certain elements of a scenario, and to estimate the magnitude of the errors committed while performing the campaign. The results of this study have been compared with real data coming from an early measuring campaign performed by the Sardinia Radio Telescope (SRT) on 04/17/2016.

Space Debris are manmade objects with variable size and shape orbiting around Earth, including satellite fragments, rocket stages and other objects that have stop their functions [1]. Such objects represent a considerable problem for future human space activities. Although space debris populate three different types of orbit, LEO (Low Earth Orbit, between 160 and 2˙000 km), MEO (Medium Earth Orbit, between 6˙000 and 12˙000 km) and GEO (Geostationary Earth Orbit, 36˙000 km), the main focus for space debris monitoring and study is the first one, due to the maximum concentration of objects. The number and typology of the orbiting debris is catalogued by the US Space Surveillance Network: around 30˙000 objects with a Radar Cross Section (RCS) larger than 10 cm, 750˙000 larger than 1 cm and more than 166 million larger than 1 mm [2]. With such a heavily congested environment it is clear that the chances of a collision are very high. The existing countermeasures for this particular problem comprehend collision avoidance maneuvers, typically for objects larger than 10 cm, while for smaller objects is preferred a shielding solution [3]. The collision avoidance is granted by frequent observation of the debris phenomenon. These observations can be realized in terms of ground-based (radar and optical) or space-based measurements [3].

In this study the authors performed a deep analysis of the input parameters concerning a bistatic radar scenario for space debris detection purposes. The results of the analysis have been compared with real measures made during the 17th April 2014 campaign.

2. ACRONYMS AND DEFINITIONS

CW – Continuous Wave
ESA – European Space Agency
FTS – Flight Termination System
FOV – Field of View
GEO – Geostationary Earth Orbit
INAF – Istituto Nazionale di Astrofisica
LEO – Low Earth Orbit
MASTER – Meteoroid and Space Debris Terrestrial Environment Reference
MEO – Medium Earth Orbit
OAC – Osservatorio Astronomico di Cagliari
PISQ – Poligono sperimentale e di addestramento Interforze di Salto di Quirra
PROOF – Program for Radar and Optical Observation Forecasting
RCS – Radar Cross Section
SNR – Signal to Noise Ratio
SRT – Sardinia Radio Telescope
SSA – Space Situational Awareness
SSN – Space Surveillance Network
TLE – Two-Line Element Set
UHF – Ultra High Frequency

3. SPACE DEBRIS CHARACTERISTICS

Space debris are all the inactive human-made orbiting objects, including fragments. In near-Earth space, this debris is more significant than natural meteoroids, except around millimeter sizes, where meteoroids prevail in some orbital regions.

Considering a typical velocity of 10 km/s in LEO (about 15 times the projectile speed), a collision between a space debris larger than about 10 cm with an operative object, it could cause a catastrophic break-ups like the spacecraft destruction. The consequence can be a cascading process, the so called 'Kessler syndrome', in which each collision between objects generates more space debris, which increases the likelihood of further collisions. Collisions with debris larger than 1 cm could disable an operational satellite or could cause the break-up of a satellite or rocket body. Impacts by millimeter-sized objects could cause local damage or disable a subsystem of an operating satellite.

A space debris is characterized by a Two-line Element set (TLE). This is a data format encoding a list of orbital elements of an Earth-orbiting object for a given point in time: the epoch. The definition of Two-line Element set coordinate system is the following:

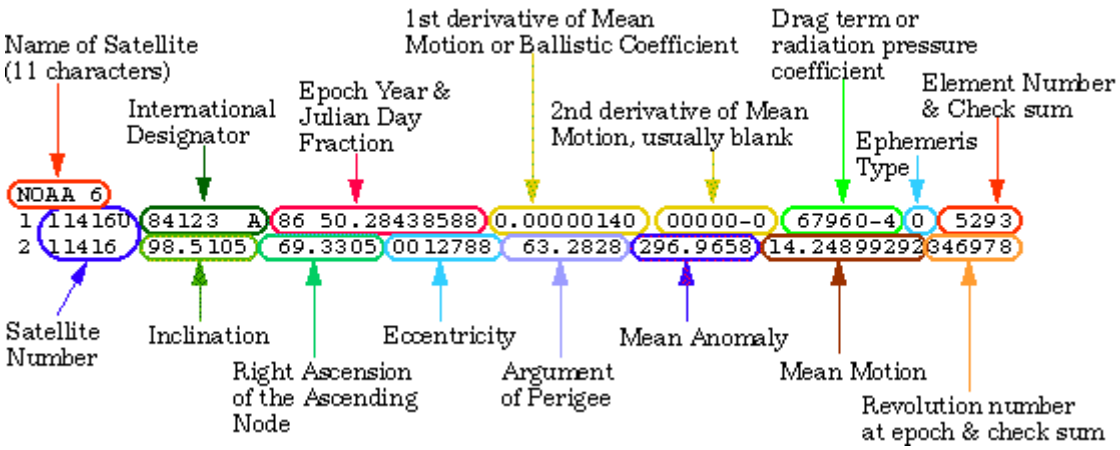

where:

- Name of Satellite (NOAA 6) represents simply the name associated with the satellite;
- International Designator (84 123A) where the 84 indicates launch year was in 1984, while the 123 tallies the 124th launch of the year, and "A" shows it was the first object resulting from this launch;
- Epoch Date and Julian Date Fraction is just the number of days passed in the particular year;
- Ballistic Coefficient (0.00000140) is the daily rate of change in the number of revs the object completes each day, divided by 2 (units are revs/day);
- Second Derivative of Mean Motion consist of a second order drag term in the SGP4 predictor used to model terminal orbit decay;

- Drag Term, (67960-4 = 0.000067960) also called the radiation pressure coefficient (or BSTAR), the parameter is another drag term in the SGP4 predictor;
- Element Set Number and Check Sum (5293) is a running count of all 2 line element sets generated by USSPACECOM for this object (in this example, 529);
- Satellite Number (11416) represents the catalog number USSPACECOM has designated for this object;
- Inclination (degrees) is the angle between the equator and the orbit plane;
- Right Ascension of the Ascending Node (degrees) is the angle between vernal equinox and the point where the orbit crosses the equatorial plane (going north);
- Eccentricity (0012788) consist of a constant defining the shape of the orbit (0=circular, Less than 1=elliptical);
- Argument of Perigee (degrees) is the angle between the ascending node and the orbit's point of closest approach to the earth (perigee);
- Mean Anomaly (degrees) is the angle, measured from perigee, of the satellite location in the orbit referenced to a circular orbit with radius equal to the semi-major axis;
- Mean Motion (14.24899292) is the mean number of orbits per day the object completes;
- Revolution Number and Check Sum (346978) represents the orbit number at Epoch Time.

The TLE of space debris observed are the following:

```
0 COSMOS 2237
1 22565U 93016A   14106.09855766  .00000097  00000-0  78836-4 0  9999
2 22565 070.8576 328.2622 0004269 357.4521 167.0091 14.12416425 85960
0 HJ-1A
1 33320U 08041A   14106.19578794 -.00000990  00000-0 -13816-3 0  9998
2 33320 098.0852 164.5031 0028792 147.3514 213.0229 14.75109358301947
0 CARTOSAT 2A
1 32783U 08021A   14106.47779497  .00001647  00000-0  23127-3 0  9996
2 32783 097.9454 166.9575 0014503 102.1684 258.1154 14.78685515322055
0 COSMOS 1408
1 13552U 82092A   14106.47516909  .00005172  00000-0  26011-3 0  9998
2 13552 082.5730 353.9271 0024505 142.8687 272.6041 15.16746691720978
0 COSMOS 1375 DEB
1 16206U 82055H   14106.85305537  .00000064  00000-0  15580-3 0  9995
2 16206 065.8365 351.3659 0012249 034.7892 017.4103 13.72968735596369
0 VESSELSAT 2
1 38047U 12001B   14106.13700250  .00014751  00000-0  41645-3 0  9997
2 38047 097.4169 193.1582 0006910 232.1981 191.1685 15.36454429126486
```

The linear speed of every debris in Table I is calculated from TLE Mean Motion data and compared with the velocity information from SGP4 propagator results.

TABLE I – Comparison between debris speed obtained from TLE and from SGP4.

Debris	Altitude [km]	TLE speed [km/s]	SGP4 speed [km/s]
COSMOS 2237	853	7.43	7.43
HJ-1A	630	7.60	7.56
CARTOSAT 2A	630	7.54	7.55
COSMOS 1408	524	7.61	7.60
COSMOS 1375	984	7.35	7.37
VESSELSAT 2	462	7.64	7.64

4. RADAR CONFIGURATION

The radar configuration studied it is bistatic where the transmitter and receiver antennas are separated. In particular, the transmitter is represented by the "Flight Termination System" (FTS) of Italian Joint Test Range located in Salto di Quirra (PISQ) at Lat. 39.493068° - Long. 9.64308°, and the receiver is represented by the Sardinia Radio Telescope (SRT) located 35 km north of Cagliari (San Basilio) at Lat. 39.49307238896° - Long. 9.2451512445321°. It is an architecture used in tracking mode and the name is BIRALET (BIstatic RAdar for LEo Tracking). Since the FTS is a military facility, the information about the radar are difficult to obtain, so for this study the authors made some hypothesis that could not be entirely exact. The FTS, owned by Italian Air Force, consists of a powerful amplifier capable to supply an averaged and leveled power of 4 kW in the 400-455 MHz bandwidth [4]. The transducers used by the FTS are an omnidirectional antenna and a wide beam directional antenna (hypothetically a 7-mt diameter antenna [5]). The transmitter is usually employed in CW mode and consequently prevent the ability to measure the object range. The receiver is the 64-mt dish Sardinia Radio Telescope, a fully steerable wheel-and-track parabolic antenna. In full operational mode SRT is able to host up to 20 remotely controllable receivers and to observe the sky with high efficiency in the frequency range between 0.3-116 GHz [6].

The first step is to calculate the gain of the transmitter-receiver system using the following formula:

$$G_{T_{[dB]}} = 10\log_{10}\left(\frac{4\pi}{\lambda^2}A_{eff}\right) = 10\log_{10}\left(\frac{4\pi}{\lambda^2}\,\eta\frac{\pi d^2}{4}\right) \qquad (3.1)$$

where λ is the wavelength, A_{eff} is the effective area of the antenna, d the antenna diameter and η his efficiency. The working frequency of the system is set at 410 MHz (λ = 0.732 m). In this configuration, the transmitter antenna cannot behave as an efficient reflector, because the diameter of the dish is shorter than 10 λ, consequentially we assume that the antenna efficiency is not very high (~20%). Concerning the receiver antenna, on the basis of data from SRT project book [6], the efficiency revolves around 60%. By applying the equation 3.1, the obtained gains for the transmitter and the receiver are respectively 22.6 dBi and 46.5 dBi.

5. RADAR EQUATION

Starting from scratch is always good to rely on theoretical basis. It is quiet easy to calculate the power received by SRT in our case by applying the well known radar equation for the bistatic configuration in a Matlab script:

$$P_R = \frac{P_T G_T G_R \lambda^2 \sigma}{(4\pi)^3 R_T^2 R_R^2} \qquad (4.1)$$

where P_R is the received power, P_T the transmitted power, G_T the transmitter antenna gain (calculated as in eq. 3.1), G_R the receiver antenna gain, λ the wavelength, σ the radar cross section, R_T the distance of the object from the transmitter and R_R the distance of the object from the receiver.

The received power (in dBm) has been evaluated in two cases:

- Fixing RCS to 1 cm^2 and varying the range (assuming R_T=R_R) between 200 and 2000 km (fig.1); for higher RCS the curve is obviously shifted along y-axis by a positive value (e.g. +10 dB for 1 cm^2 RCS and +30 dB for 1 m^2 RCS).
- Fixing range to 200 km (assuming R_T=R_R) and varying the RCS between 1 cm^2 and 20 m^2 (fig. 2); for higher ranges the curve is shifted along y-axis by a negative value (e.g. -30 dB for 1000 km range and -40 dB for 2000 km range).

As expected, due to the direct proportion, the received power decrease with the range increment (fig. 1) and contextually increase with the RCS decrement as a result of the inverse proportionality (fig. 2).

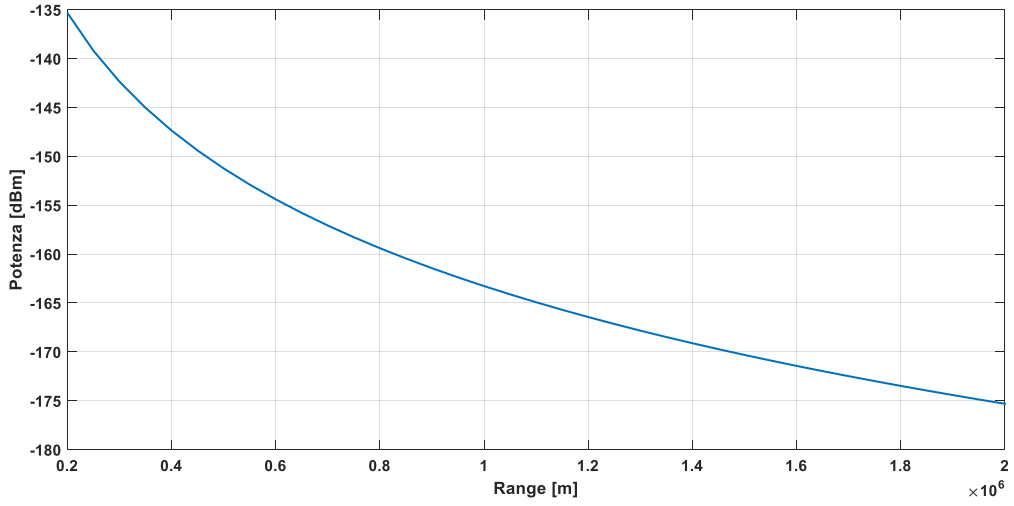

FIGURE 1 - Received power from a 1 cm^2 RCS debris and varying the range between 200 and 2000 km.

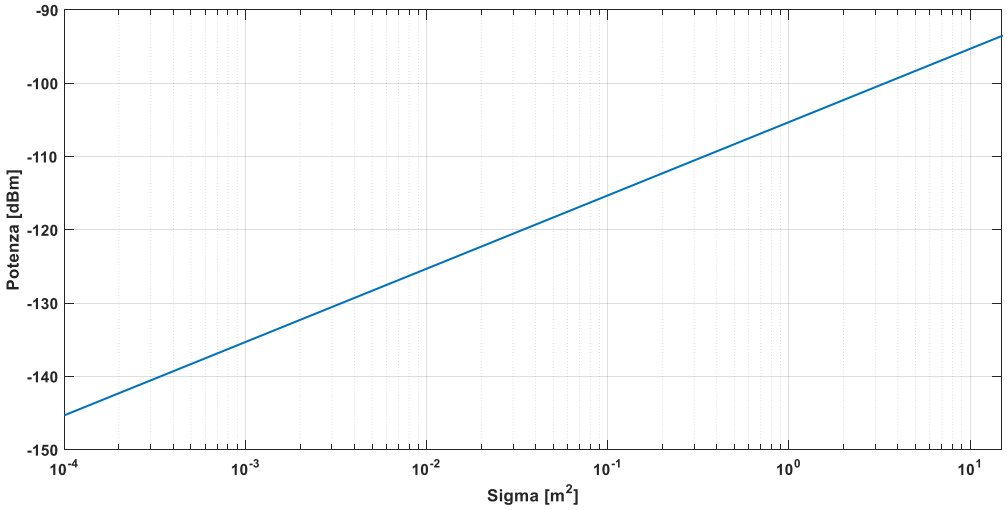

FIGURE 2 - Received power for 200 km range and variable RCS between 1 cm^2 and 20 m^2.

6. SNR PROFILES

Probably the most important parameter to evaluate is the Signal-to-Noise Ratio (SNR), which represent the logarithmic power ratio between the received signal and the noise and is defined by the following equation:

$$SNR = \frac{P_T G_T G_R \lambda^2 \sigma \tau}{(4\pi)^3 R_T^2 R_R^2 k T_s L} \tag{5.1}$$

where τ is the pulse width and is the inverse of the bandwidth of the signal, k is the Boltzmann constant, $T_s = TF_n$ is the system temperature (product of temperature T and noise factor F_n) and L is the path loss. Since, as already mentioned in the introduction, the transmitted signal is a CW, in this case we used, as τ, the expected time in which the debris crossed the illuminated area by BIRALET (around 0.5 seconds).

The list of the space debris to detect, complete with RCS, range and time of passage, has been provided by Italian Air Force and is shown in the following Table II.

TABLE II - List of the debris with RCS, range from FTS and SRT and FTS turn-on and turn-off time.

Name	ID	RCS [m^2]	Range from FTS [km]	Range from SRT [km]	Start time [UTC]	Stop time [UTC]
COSMOS 2237 (first passage)	22565	11.64	865	867	08:22:40	08:23:00
COSMOS 2237 (second passage)	22565	11.66	1384	1452	08:25:30	08:25:50
HJ-1A (first passage)	33320	1.497	1842	1798	08:56:33	08:56:53
HJ-1A (second passage)	33320	1.497	930	902	08:59:00	08:59:20
CARTOSAT 2A	32783	2.341	1023	1033	09:10:50	09:11:10
COSMOS 1408	13552	8.4523	542	551	09:30:05	09:30:15
COSMOS 1375	16206	0.485	1185	1141	10:23:30	10:23:50
VESSELSAT 2	38047	0.2822	854	810	10:51:30	10:51:50

Using a simple script in Matlab we were able to obtain the SNR of the above mentioned debris. The function, already present in the Matlab Phased Array Toolbox (http://it.mathworks.com/help/phased/ref/radarequationcalculator.html), is radareqsnr () that estimates the output signal-to-noise ratio (SNR) at the receiver based on the wavelength in meters, the range in meters, the peak transmit power in watts, and the pulse width in seconds. The input parameters were the same used for the radar equation in section 4, except for the pulse width (0.5 seconds), the system temperature (60 K) and the path loss (2 dB). The output of the script is shown in Table III.

TABLE III - SNR of the debris evaluated with the Matlab script.

Name	ID	SNR [dB]
COSMOS 2237 (first passage)	22565	48.43
COSMOS 2237 (second passage)	22565	39.87
HJ-1A (first passage)	33320	26.62
HJ-1A (second passage)	33320	38.55
CARTOSAT 2A	32783	38.48
COSMOS 1408	13552	55.04
COSMOS 1375	16206	29.51
VESSELSAT 2	38047	32.97

This results will be commented in section 12 and compared with the real SNR profiles measured during 17th April campaign.

7. RADAR DOPPLER FREQUENCY

In order to evaluate the Doppler shift frequency of the debris, the following formula was used [8]:

$$\Delta f = \frac{1}{\lambda}(v \cdot \hat{\rho}_{TX} + v \cdot \hat{\rho}_{RX}) \tag{6.1}$$

where v is the debris velocity, $\hat{\rho}_{TX}$ and $\hat{\rho}_{RX}$ are the versors of the conjunction vectors between the transmitter (FTS) and the target and the receiver (SRT) and the target, respectively, in agreement with figure 3.

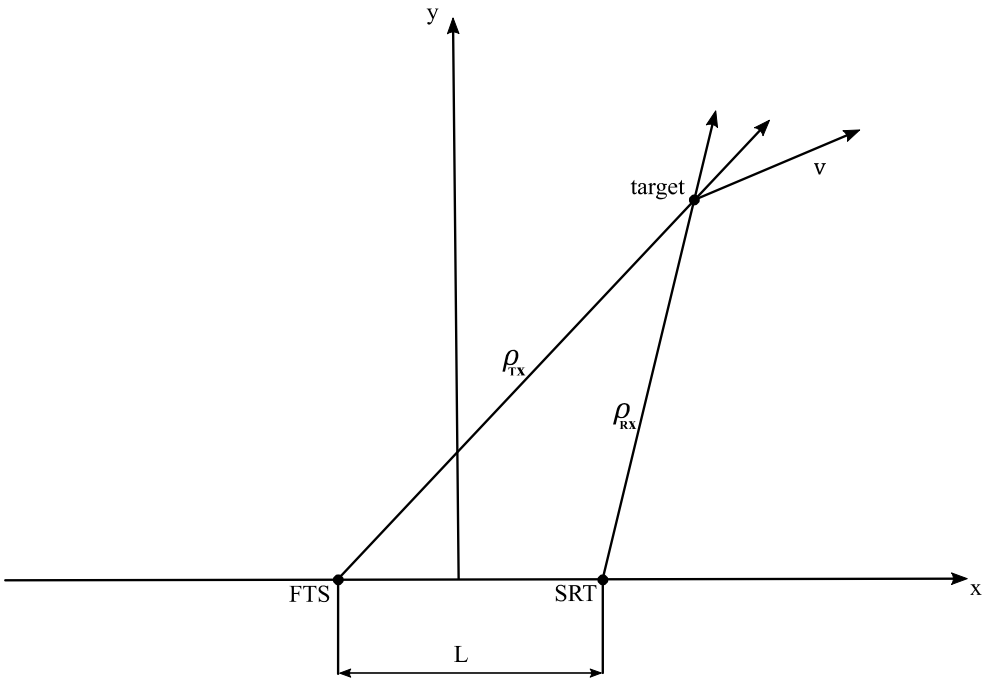

FIGURE 3 - Bistatic Doppler scenario.

To obtain coherent results, the whole system has been implemented in a single coordinate system, the Earth-Centered Earth-Fixed (ECEF). This coordinate system rotates with the earth around its spin axis. As such, a fixed point on the earth surface has a fixed set of coordinates (Fig. 4).

The origin and axes of the ECEF coordinate system are defined as follows:

1. The origin is located at the center of the earth.
2. The Z-axis is along the spin axis of the earth, pointing to the north pole.
3. The X-axis intersects the sphere of the earth at 0° latitude and 0° longitude.

4. The Y-axis is orthogonal to the Z- and X-axes with the usual right-hand rule.

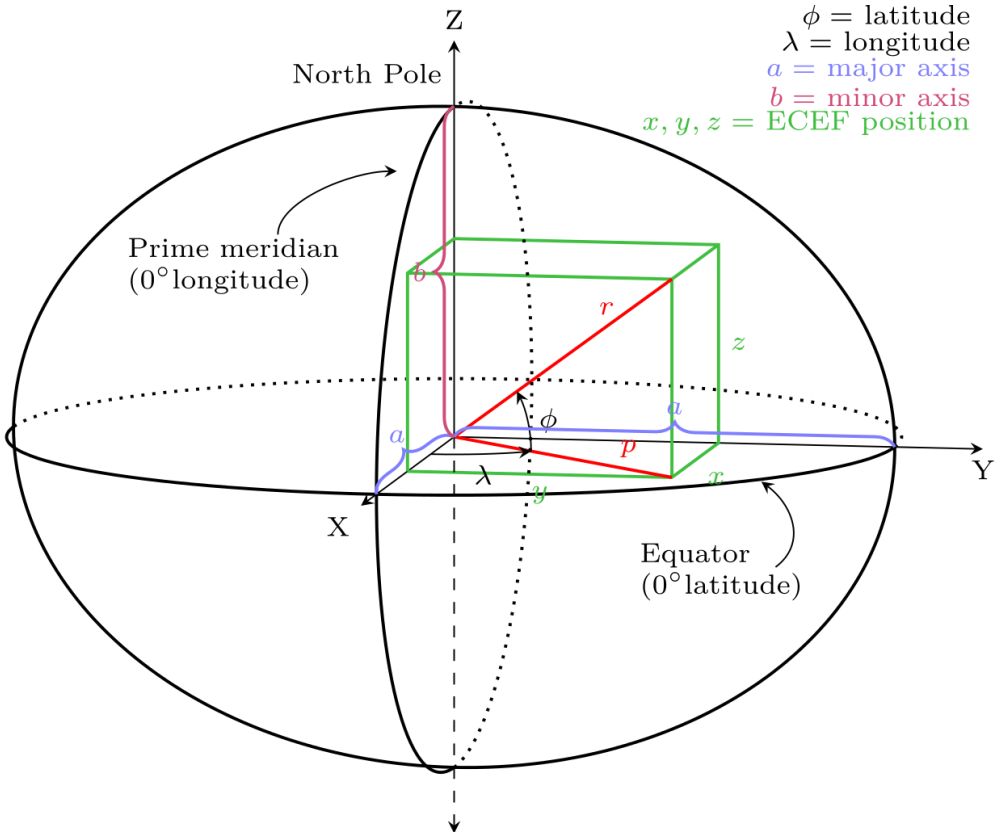

FIGURE 4 - The ECEF coordinate system.

Coordinate vectors expressed in the ECEF frame are denoted with a subscript e. Similar to the geodetic system, the position vector in the ECEF frame is denoted by:

$$P_e = \begin{pmatrix} x_e \\ y_e \\ z_e \end{pmatrix} \tag{6.2}$$

therefore, the altitude, longitude and latitude of FTS and SRT were converted in ECEF coordinates.

As regards the state of debris (position and velocity of the object), the Simplified General Perturbations (SGP4) propagator is used with two-line element (TLE) sets. It considers secular and periodic variations due to Earth oblateness, solar and lunar gravitational effects, gravitational resonance effects, and orbital decay using a drag model. SGP4 allows to obtain the state of debris in Earth-Centered Inertial (ECI) coordinate system. The ECI coordinate system (see Figure 5) is typically defined as a Cartesian coordinate system, where the coordinates (position) are defined as the distance from the origin along the three orthogonal (mutually perpendicular) axes. The z axis runs along the Earth's rotational axis pointing North, the x axis points in the direction of the vernal

equinox (more on this in a moment), and the y axis completes the right-handed orthogonal system. As seen in Figure 5, the vernal equinox is an imaginary point in space which lies along the line representing the intersection of the Earth's equatorial plane and the plane of the Earth's orbit around the Sun or the ecliptic. Another way of thinking of the x axis is that it is the line segment pointing from the center of the Earth towards the center of the Sun at the beginning of Spring, when the Sun crosses the Earth's equator moving North. The x axis, therefore, lies in both the equatorial plane and the ecliptic. These three axes defining the Earth-Centered Inertial coordinate system are 'fixed' in space and do not rotate with the Earth.

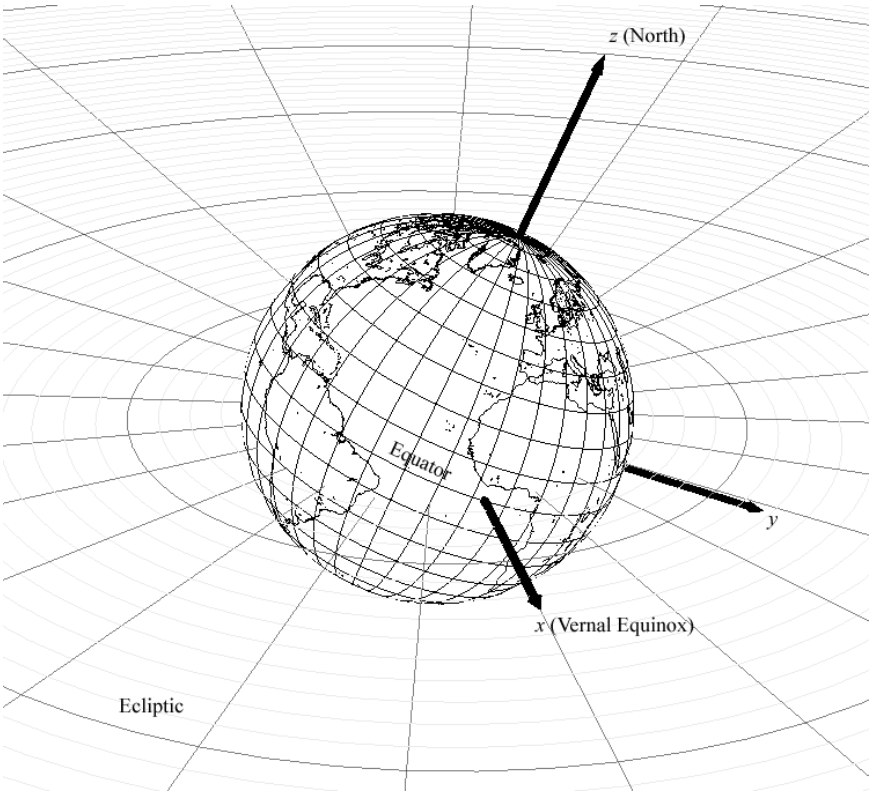

FIGURE 5 - The ECI coordinate system.

Then, the position and velocity of the space debris have been converted from ECI to ECEF. In this way every single object in the scenario shared a common reference system.

The Doppler shift values obtained (with a Matlab script) are summarized in Table IV and will be compared with the real values reported in section 10.

TABLE IV – Simulated Doppler shift values.

Name	ID	Doppler shift [kHz]
COSMOS 2237 (first passage)	22565	- 0.431
COSMOS 2237 (second passage)	22565	-15.356
HJ-1A (first passage)	33320	+17.984
HJ-1A (second passage)	33320	+12.850
CARTOSAT 2A	32783	+14.663
COSMOS 1408	13552	-0.991
COSMOS 1375	16206	+9.306
VESSELSAT 2	38047	+18.875

8. AZIMUTH AND ELEVATION POINTING ANGLES

The azimuth and elevation pointing angles were obtained using a Python script, which takes the TLEs of the debris and the UTC time of observation in input and gives the pointing coordinates, expressed in degrees to the third decimal place, in output. The resulting azimuth and elevation coordinates are shown in Table V.

TABLE V – Azimuth and Elevation pointing angles calculated with the Python script.

Name	Azimuth (deg)	Elevation (deg)
COSMOS 2237 (first passage)	109.779	79.253
COSMOS 2237 (second passage)	28.829	31.028
HJ-1A (first passage)	18.834	13.501
HJ-1A (second passage)	32.789	42.209
CARTOSAT 2A	22.763	36.993
COSMOS 1408	92.120	71.059
COSMOS 1375	204.524	57.018
VESSELSAT 2	30.764	32.009

Before starting the simulations the authors already knew that for the 2014 observation campaign the azimuth and elevation coordinates were obtained using the software WXtrack, which has a lower precision. This may lead to an error in SNR evaluation, that will be discussed in section 11.

9. ESA MASTER AND PROOF

In order to forecast the possible debris detections, the ESA PROOF (Program for Radar and Optical Observation Forecasting) 2009 software has been used. PROOF 2009 is a software developed by European Space Agency for the simulation of radar- and telescope-based space debris observation. This software can be a useful tool, in order to plan space debris observation campaigns and validate previous campaigns. Every run of PROOF need specific parameters, mostly tied to geographical coordinates and operational settings of the radars or telescopes in use (i.e. work frequency, beam width, transmitted power, etc.) and to observation epoch. It is worth mentioning that PROOF cannot run properly without an up to date debris population file, which describes the distribution of objects at a given astronomic epoch. Obviously the observation epoch must be as close as possible to the epoch of the population file. Unfortunately, the PROOF database provides population files update to 1st May 2009, so that simulations carried out after this particular date could be inaccurate. This is the main reason why PROOF shouldn't be used without the support of ESA MASTER (Meteoroid and Space Debris Terrestrial Environment Reference Model) 2009, a software for characterization of the natural and man-made particulate environment of the Earth. MASTER database is constantly updated and it can be used by PROOF to "propagate" the last population file available up to the requested epoch.

Once the list of debris and the time of illumination are available, it's necessary to obtain the pointing angles (azimuth and elevation) of the radar/s or telescope/s and for the specific case of the BIRALET bistatic radar system, two sets of angles are needed, one for the FTS and one for the SRT respectively. In order to get the above mentioned angles, WXtrack has been used, a free software for amateur users, which allows to set the observing location with its Latitude, Longitude, Height and minimum elevation. The remaining input parameters are basically related to the radars.

Figure 6 shows that, for the given configuration, there is a very large number of objects, located at altitudes between 600 km and about 2000 km (LEO), that cross the illuminated area. However, the red line means that they can't be detected, probably due to their small dimension. Nevertheless there is a significant amount of objects, represented by a light blue line (which identify the TLE objects), that cross the illuminated area and that can be detected with the given configuration. Similar results can be obtained also considering other parameters (diameter, range, RCS, etc.). It is also possible to identify a particular debris among the others. Let's take for example the debris 22565 (COSMOS 2237), which has afterwards been successfully detected by the BIRALET configuration. According to WXtrack this very specific debris could have been detected at 08:22:40 of 2014/04/17 (the observation date) pointing the FTS toward

144.8° Az and 79.3° El and the SRT toward 109.8° Az and 79.3° El, at a range of about 866 km from both transmitter and receiver. From the TLE it is possible to extract the semi major orbit axis, which for COSMOS 2237 happens to be equal to about 7200 km. In figure 7 it is pretty clear the detection of the COSMOS 2237.

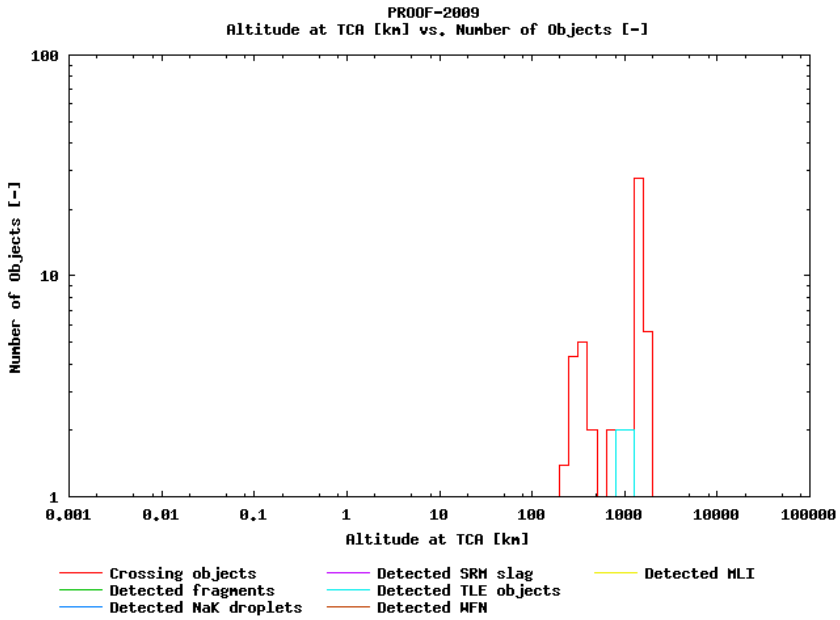

FIGURE 6 - Number of crossing (red line) and detected (light blue line) for the BIRALET configuration.

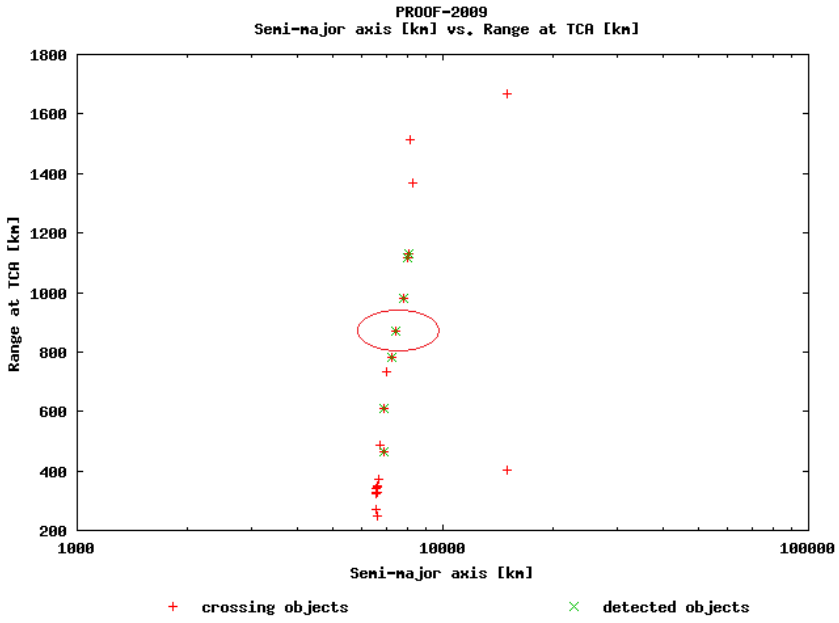

FIGURE 7 - Detection of the COSMOS 2237.

10. SPACE DEBRIS DETECTION CAMPAIGN ON 2014/04/17

Phase 2 of the AM-INAF agreement on Space Situational Awareness (SSA) included a set of measures in the UHF band for LEO space debris observation. The radars used for this purpose were, as already sad, the BIRALET system, with the FTS as transmitter and the SRT as receiver. After a preliminary test in 04/14/2014, three days later the real detection campaign has begun. During this session, a sinusoidal signal (CW) of about 4 kW has been transmitted from the FTS to the identified debris and observed both by the Medicina's Northern Cross and the Sardinia Radio Telescope. The session objectives for SRT were:

- Target revelation (SNR), acquisition time and radar echo loss;
- Measurement of the relative target speed.

The backend used during the sessions were at first the HP 8594E spectrum analyzer for the preliminary test on April 14th and then the Agilent A4446E with the following setup:

- FFT mode;
- Span 100 kHz (200 kHz for the detection of COSMOS 2237);
- Resolution Bandwidth 200 Hz (400Hz for the detection of COSMOS 2237) with 500 points;
- Video Bandwidth 200 Hz.

Moreover, for almost every tests (except for the detection of VESSELSAT 2) an amplificator with 25 dB gain was added to the measure set-up setting an attenuation of the spectrum analyzer equal to 10 dB, for a total value of 15 dB.

The list of the debris is the same of Table I. As it can be read from the table for almost every debris the total switching on interval of the transmitter was 20 seconds, 10 seconds before and 10 seconds after the debris crossed the space volume observed. For every object, Table VI shows the name and passage of the debris, the duration of the received echoes, the Doppler shift and the SNR.

TABLE VI - Duration, Doppler frequency and SNR of the detected debris.

Name	Duration [s]	Doppler frequency [kHz]	SNR [dB]
COSMOS 2237 (first passage)	0.440	Doppler not measured	39.8
COSMOS 2237 (second passage)	0.473	-5.2	29.4
HJ-1A (first passage)	0.305	+6.2	16.4
HJ-1A (second	0.380	+4.6	15.8

passage)			
CARTOSAT 2A	0.296	+5.2	11.7
COSMOS 1408	0.507	Doppler not measured	37.2
COSMOS 1375	0.414	+3.4	10.8
VESSELSAT 2	0.390	+5.2	17.4

The spectrograms of the 20 seconds window are plotted in the next pages (21-28), showing the level of the received power as a function of time and frequency. From these images it is possible to notice the received power at SRT and the Doppler frequency shift.

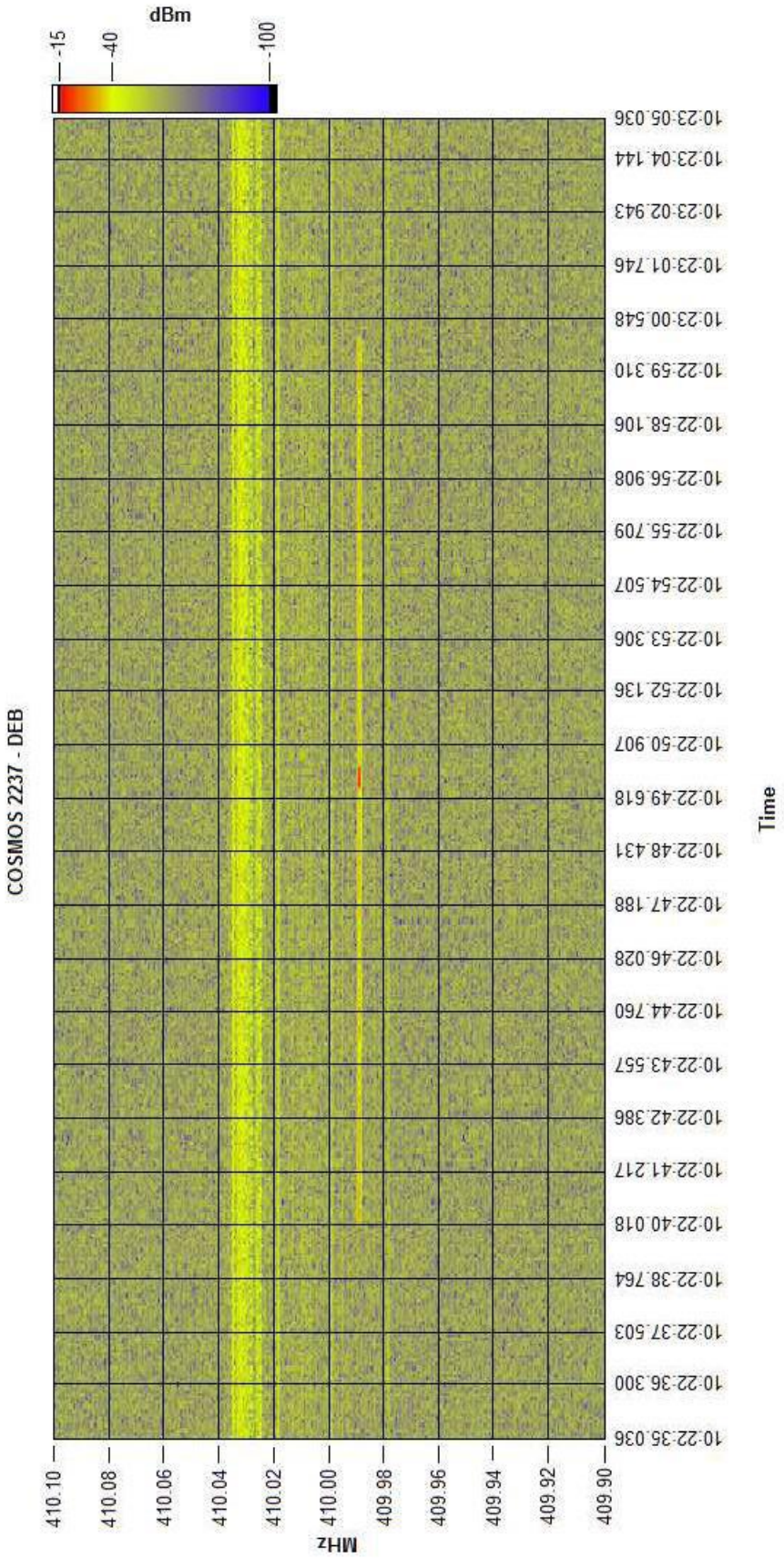
dBm
-15
-40
-100
COSMOS 2237 - DEB
Time
10:23:05.036
10:23:04.144
10:23:02.943
10:23:01.746
10:23:00.548
10:22:59.310
10:22:58.106
10:22:56.908
10:22:55.709
10:22:54.507
10:22:53.306
10:22:52.136
10:22:50.907
10:22:49.618
10:22:48.431
10:22:47.188
10:22:46.028
10:22:44.760
10:22:43.557
10:22:42.386
10:22:41.217
10:22:40.018
10:22:38.764
10:22:37.503
10:22:36.300
10:22:35.036
410.10
410.08
410.06
410.04
410.02
410.00
409.98
409.96
409.94
409.92
409.90
MHz

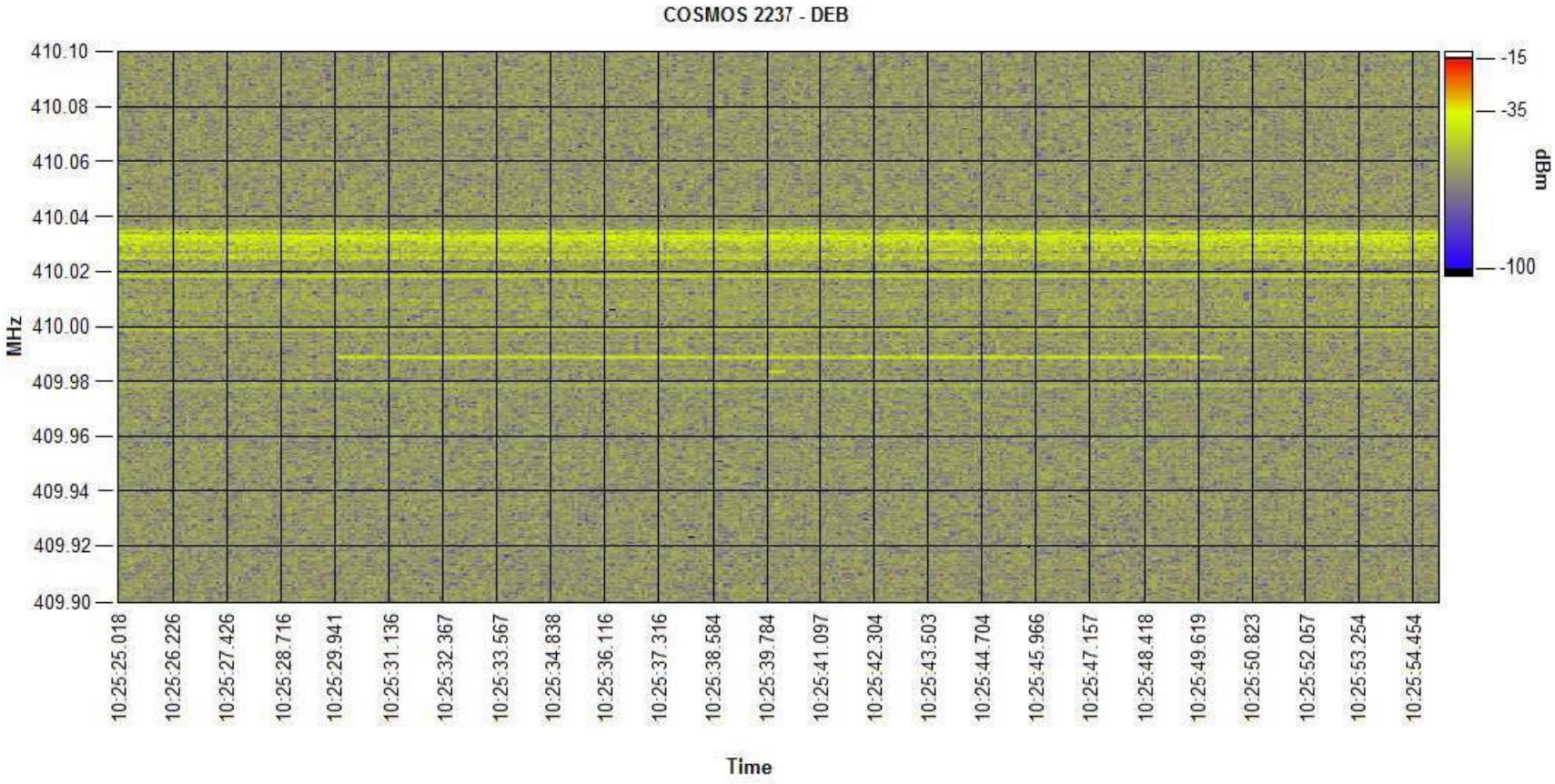
COSMOS 2237 - DEB
410.10
410.08
410.06
410.04
410.02
410.00
409.98
409.96
409.94
409.92
409.90
MHz
-15
-35
-100
dBm
10:25:25.018
10:25:26.226
10:25:27.426
10:25:28.716
10:25:29.941
10:25:31.136
10:25:32.367
10:25:33.567
10:25:34.838
10:25:36.116
10:25:37.316
10:25:38.584
10:25:39.784
10:25:41.097
10:25:42.304
10:25:43.503
10:25:44.704
10:25:45.966
10:25:47.157
10:25:48.418
10:25:49.619
10:25:50.823
10:25:52.057
10:25:53.254
10:25:54.454
Time

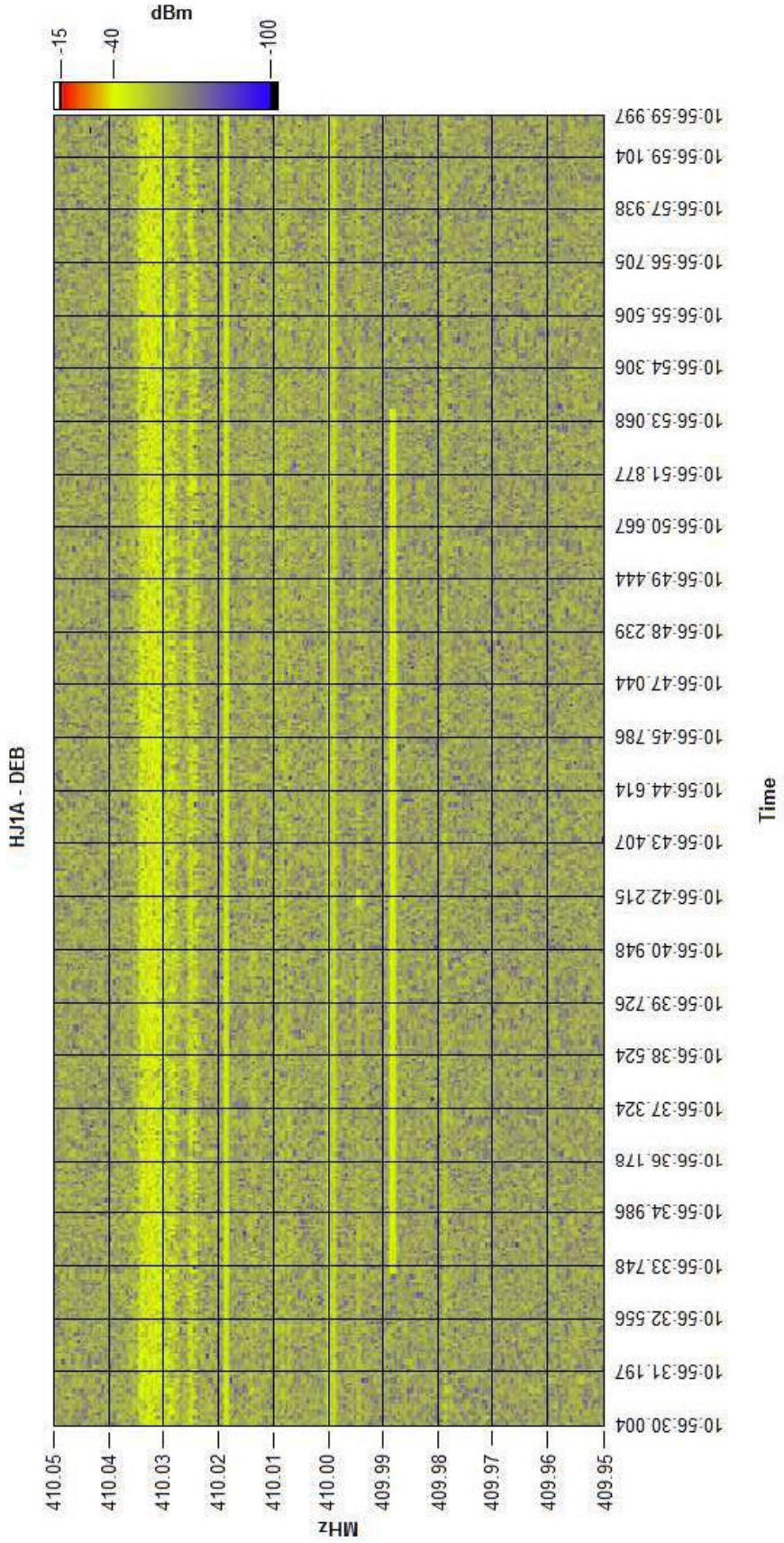
dBm
-15
-40
-100
HJ1A - DEB
Time
10:56:59.997
10:56:59.104
10:56:57.938
10:56:56.705
10:56:55.506
10:56:54.306
10:56:53.068
10:56:51.877
10:56:50.667
10:56:49.444
10:56:48.239
10:56:47.044
10:56:45.786
10:56:44.614
10:56:43.407
10:56:42.215
10:56:40.948
10:56:39.726
10:56:38.524
10:56:37.324
10:56:36.178
10:56:34.986
10:56:33.748
10:56:32.556
10:56:31.197
10:56:30.004
410.05
410.04
410.03
410.02
410.01
410.00
409.99
409.98
409.97
409.96
409.95
MHz

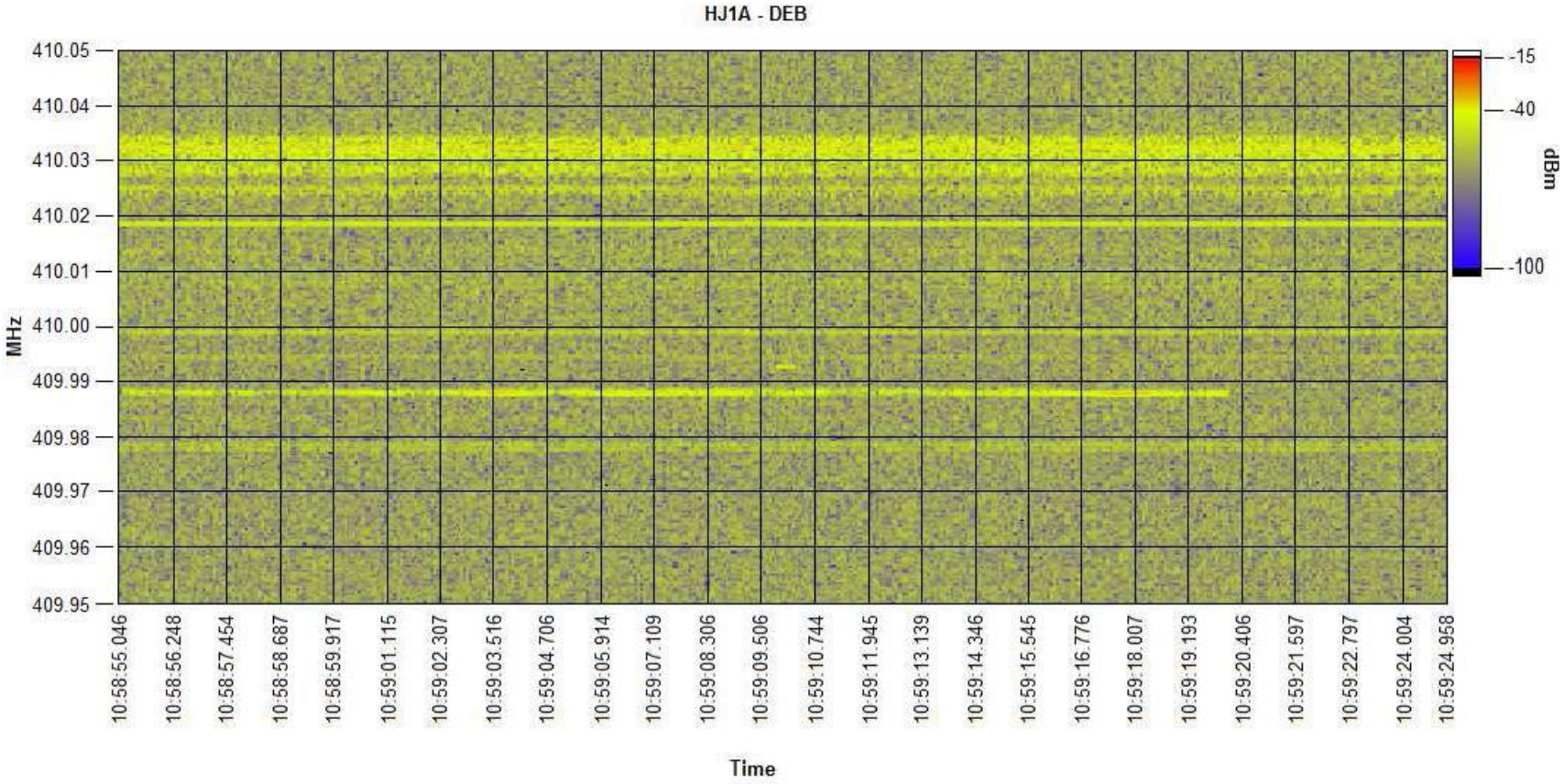
HJ1A - DEB
410.05
410.04
410.03
410.02
410.01
410.00
409.99
409.98
409.97
409.96
409.95
MHz
-15
-40
-100
dBm
10:58:55.046
10:58:56.248
10:58:57.454
10:58:58.687
10:58:59.917
10:59:01.115
10:59:02.307
10:59:03.516
10:59:04.706
10:59:05.914
10:59:07.109
10:59:08.306
10:59:09.506
10:59:10.744
10:59:11.945
10:59:13.139
10:59:14.346
10:59:15.545
10:59:16.776
10:59:18.007
10:59:19.193
10:59:20.406
10:59:21.597
10:59:22.797
10:59:24.004
10:59:24.958
Time

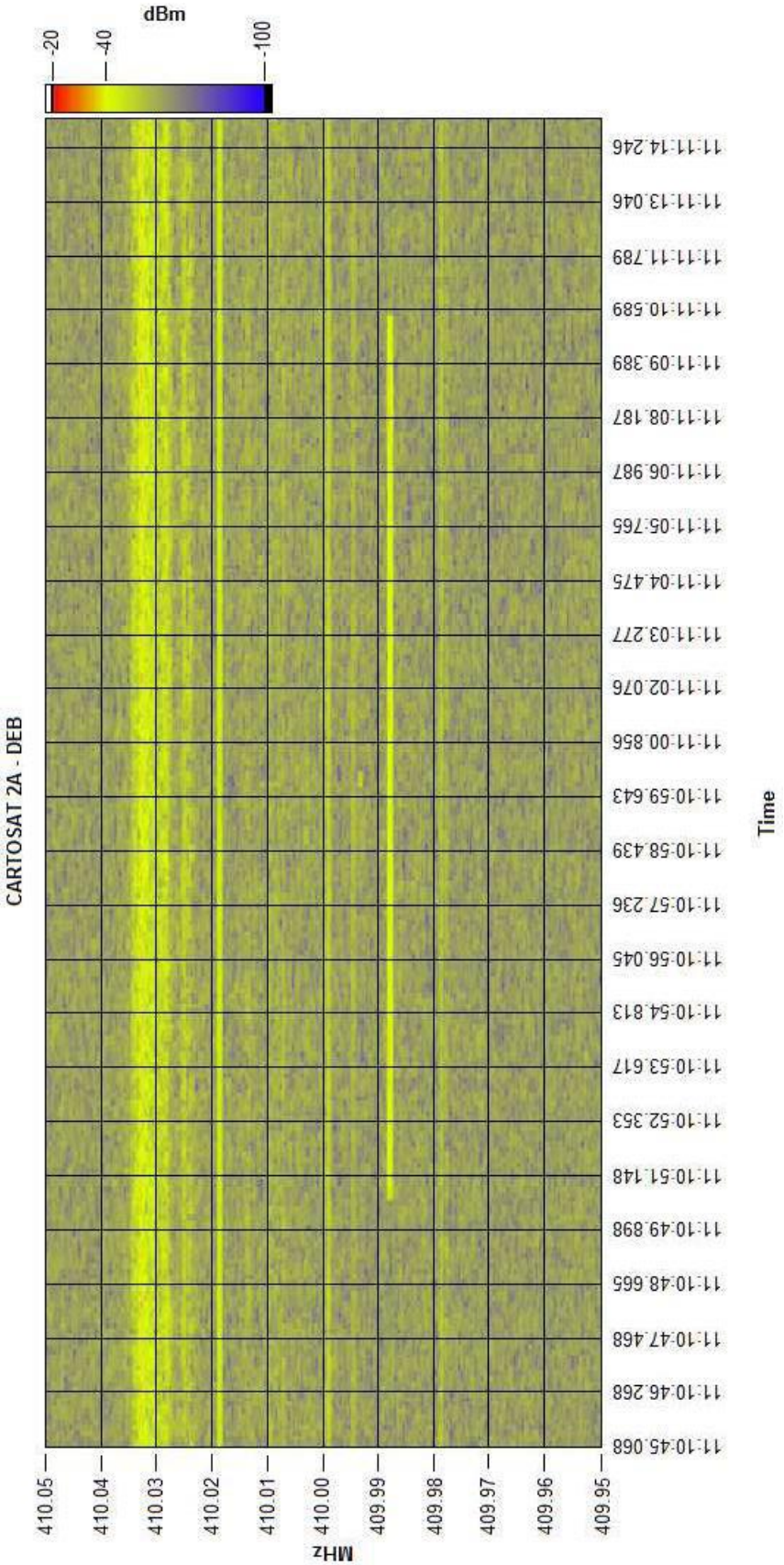
dBm
-20
-40
-100
CARTOSAT 2A - DEB
Time
11:11:14.246
11:11:13.046
11:11:11.789
11:11:10.589
11:11:09.389
11:11:08.187
11:11:06.987
11:11:05.765
11:11:04.475
11:11:03.277
11:11:02.076
11:11:00.856
11:10:59.643
11:10:58.439
11:10:57.236
11:10:56.045
11:10:54.813
11:10:53.617
11:10:52.353
11:10:51.148
11:10:49.898
11:10:48.665
11:10:47.468
11:10:46.268
11:10:45.068
410.05
410.04
410.03
410.02
410.01
410.00
409.99
409.98
409.97
409.96
409.95
MHz

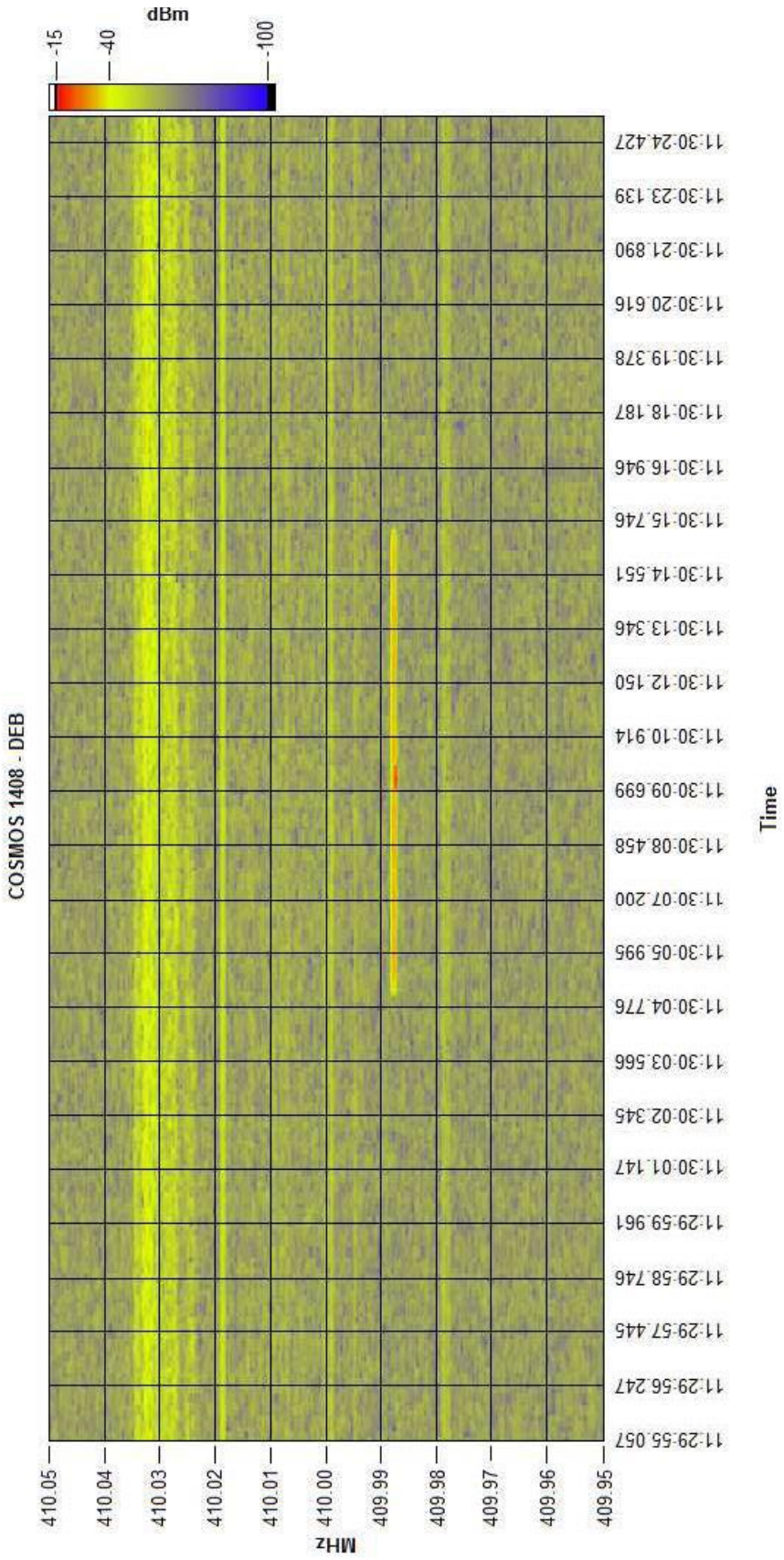
dBm
-15
-40
-100
COSMOS 1408 - DEB
Time
11:30:24.427
11:30:23.139
11:30:21.890
11:30:20.616
11:30:19.378
11:30:18.187
11:30:16.946
11:30:15.746
11:30:14.551
11:30:13.346
11:30:12.150
11:30:10.914
11:30:09.699
11:30:08.458
11:30:07.200
11:30:05.995
11:30:04.776
11:30:03.566
11:30:02.345
11:30:01.147
11:29:59.961
11:29:58.746
11:29:57.445
11:29:56.247
11:29:55.057
410.05
410.04
410.03
410.02
410.01
410.00
409.99
409.98
409.97
409.96
409.95
MHz

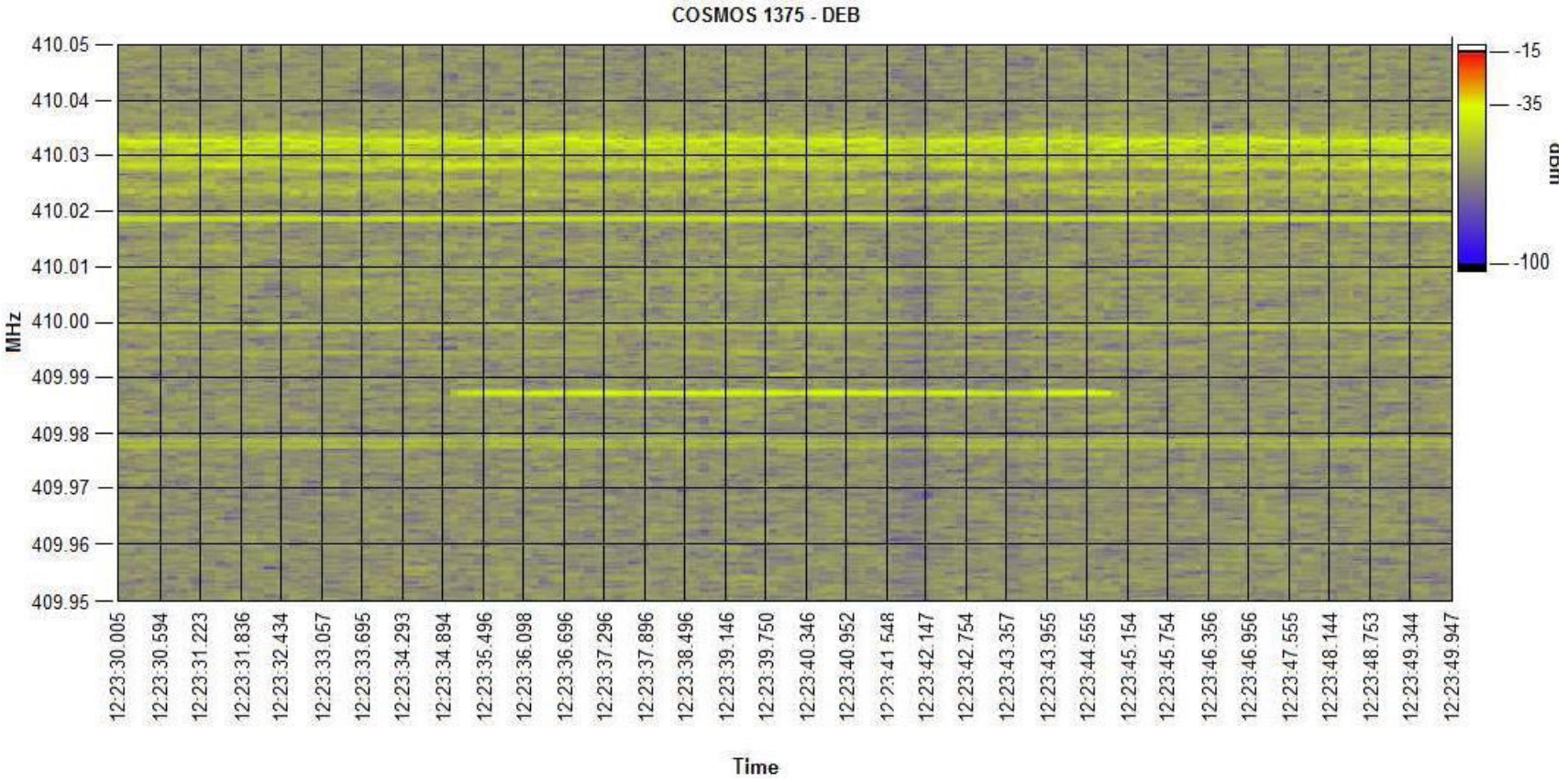
COSMOS 1375 - DEB
410.05
410.04
410.03
410.02
410.01
410.00
409.99
409.98
409.97
409.96
409.95
MHz
-15
-35
-100
dBm
12:23:30.005
12:23:30.594
12:23:31.223
12:23:31.836
12:23:32.434
12:23:33.057
12:23:33.695
12:23:34.293
12:23:34.894
12:23:35.496
12:23:36.098
12:23:36.696
12:23:37.296
12:23:37.896
12:23:38.496
12:23:39.146
12:23:39.750
12:23:40.346
12:23:40.952
12:23:41.548
12:23:42.147
12:23:42.754
12:23:43.357
12:23:43.955
12:23:44.555
12:23:45.154
12:23:45.754
12:23:46.356
12:23:46.956
12:23:47.555
12:23:48.144
12:23:48.753
12:23:49.344
12:23:49.947
Time

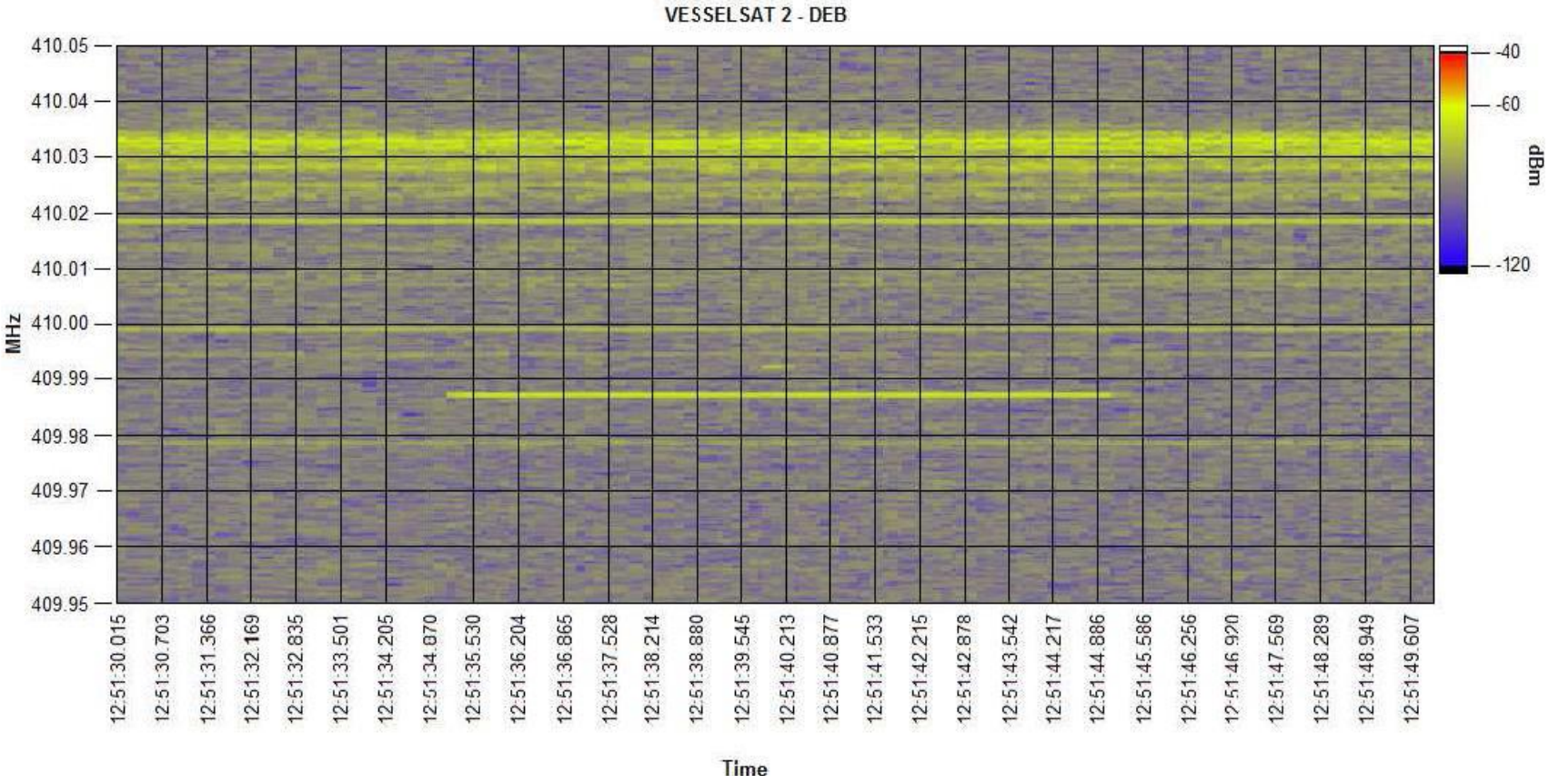
VESSELSAT 2 - DEB
410.05
410.04
410.03
410.02
410.01
410.00
409.99
409.98
409.97
409.96
409.95
MHz
-40
-60
-120
dBm
12:51:30.015
12:51:30.703
12:51:31.366
12:51:32.169
12:51:32.835
12:51:33.501
12:51:34.205
12:51:34.870
12:51:35.530
12:51:36.204
12:51:36.865
12:51:37.528
12:51:38.214
12:51:38.880
12:51:39.545
12:51:40.213
12:51:40.877
12:51:41.533
12:51:42.215
12:51:42.878
12:51:43.542
12:51:44.217
12:51:44.886
12:51:45.586
12:51:46.256
12:51:46.920
12:51:47.569
12:51:48.289
12:51:48.949
12:51:49.607
Time

11. ERROR EVALUATION

It is quite clear that there is a considerable difference between the simulated and measured data both on the SNR profiles (Fig. 8) and on the frequency Doppler shift. There is no real explanation for the error committed in the Doppler evaluation: the coordinate system has been checked several times and the calculation match perfectly with the real values of position of the FTS and the SRT and with the real values of position and speed of the debris. Moreover, the same system has been used to validate the measures of several campaigns (similar to this) done by INAF-IRA in Medicina (Bologna, Italy) with the Northern Cross, and the results are shown hereafter.

A total of six campaigns during the same year (2014) have been taken into account:

- April 14th

Name	ID	UTC	Doppler shift from Medicina dataset [kHz]	Doppler shift evaluated with the Matlab script [kHz]
SL-14 R/B	17296	12:04:45	+3.222	+2.886
YAOGAN 2	31490	12:12:13	+0.095	+0.255
SL-14 R/B	17242	12:16:12	-2.718	-2.727
NIMBUS 7	11080	12:53:00	+0.045	+0.131
THOR AGENA D R/B	2825	13:17:19	-3.430	-3.672
SL-14 R/B	15890	14:55:43	+3.508	+3.312
COSMOS 1758	16791	15:27:41	-0.146	-0.327
IRIDIUM 36	24967	15:28:13	+0.986	+0.865
CZ-4B R/B	32959	17:08:49	-6.291	-6.354
SPOT 2	20436	17:24:13	-4.243	-4.373
IRS 1A	18960	17:35:53	+2.829	+2.935

- April 15th

Name	ID	UTC	Doppler shift from Medicina dataset [kHz]	Doppler shift evaluated with the Matlab script [kHz]
TIANGONG 1	37820	13:22:37	-3.568	-4.344
COSMOS 1842	17911	13:31:26	-0.524	-0.223
SL-8 R/B	23432	13:44:31	-0.588	-0.457
SL-8 R/B	21419	13:52:17	-1.129	-0.894
CZ-2C R/B	37766	14:21:59	+2.993	+3.286
ARIANE 40 R/B	25979	14:37:24	+4.417	+4.652
H-2A R/B	33500	16:33:34	+2.165	+2.378
COSMOS 1733	16611	16:52:19	-0.365	-0.835

- April 17th

Name	ID	UTC	Doppler shift from Medicina dataset [kHz]	Doppler shift evaluated with the Matlab script [kHz]
COSMOS 2237	22565	08:23:20	+2.208	+1.599
COSMOS 1844	17973	13:31:26	-5.083	-4.758
COSMOS 1408	13552	13:44:31	+0.970	+1.691
TELKOM 3	38744	13:52:17	+2.960	+2.602
TERRA	25994	14:21:59	-4.068	-3.513

- June 4th

Name	ID	UTC	Doppler shift from Medicina dataset [kHz]	Doppler shift evaluated with the Matlab script [kHz]
CZ-2D R/B	28738	07:33:29	+0.838	+1.326
COSMOS 1707	16326	08:13:10	-0.310	-0.133
SL-8 R/B	20433	08:50:24	-3.127	-2.869
SL-24 DEB	33398	09:23:06	-1.792	-2.300
CZ-4C R/B	39014	09:40:50	+1.508	+0.944
TERRA	25994	10:11:51	-3.451	-3.088

- June 5th

Name	ID	UTC	Doppler shift from Medicina dataset [kHz]	Doppler shift evaluated with the Matlab script [kHz]
SL-8 R/B	16728	12:03:24	-7.475	-7.736
DELTA 1 R/B	20323	12:21:57	+7.273	+7.359
BREEZE-M DEB (TANK)	38654	13:04:32	+6.386	+6.807
TIANGONG 1	37820	13:35:08	-3.557	-4.267
CZ-4C DEB	39015	13:42:26	+0.109	+0.252
ARIANE 5 R/B	27387	13:46:34	+0.400	+0.103

➢ June 6th

Name	ID	UTC	Doppler shift from Medicina dataset [kHz]	Doppler shift evaluated with the Matlab script [kHz]
COSMOS 2344	24827	08:14:45	+9.002	+9.198
SL-14 R/B	21034	08:34:49	+8.273	+8.349
SL-8 R/B	15006	08:56:06	-10.293	-10.474
COSMOS 2058	20465	09:09:12	-1.385	-0.999
H-1 R/B(MABES)	16910	09:22:56	+0.026	+0.108
PSLV R/B	25759	09:26:44	-3.941	-4.328
BREEZE-M DEB	36594	09:33:12	+6.402	+5.988
SL-8 R/B	12644	09:45:48	-4.726	-5.029

In this case the error committed in the simulations is always < 1 kHz and it's probably due to the inaccuracy of the time in UTC used (the precision in the Medicina dataset was to the fraction of second and we weren't able to reach such an accuracy). However this cannot explain the huge differences in the case of the SRT simulations.

Regarding the SNR profile error, there are plenty of reasons to justify the lack of precision.

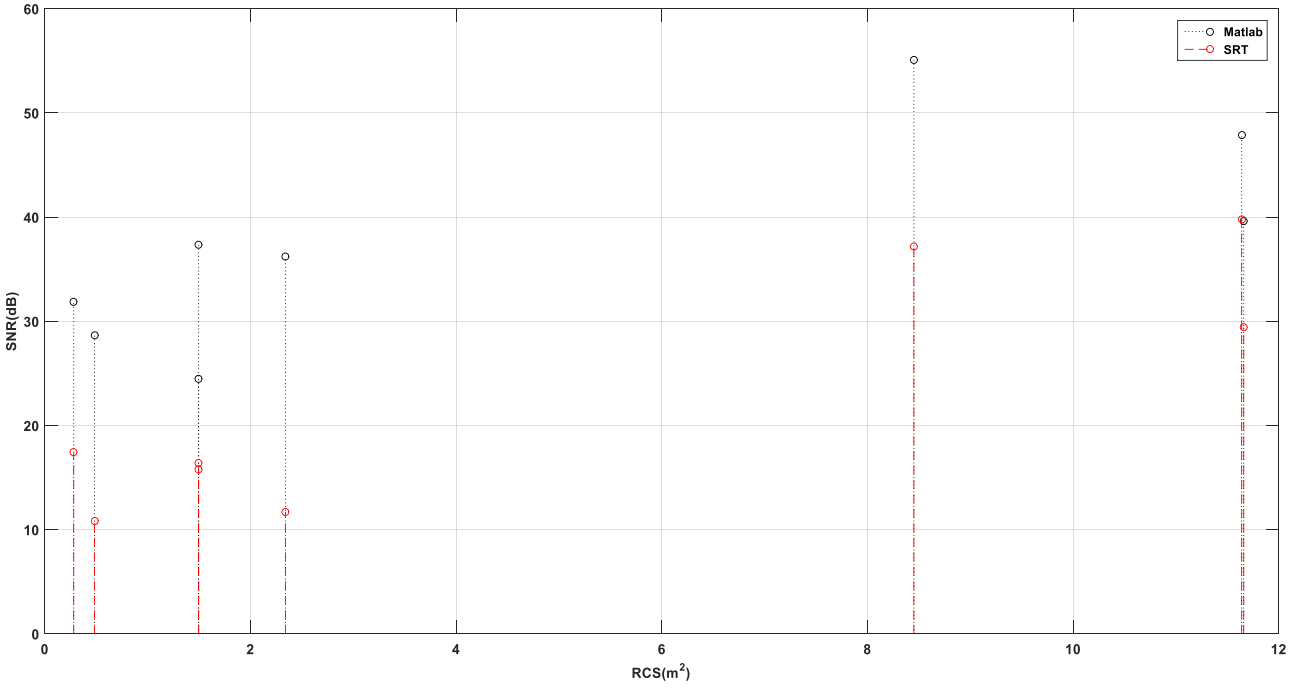

FIGURE 8 - Difference between the SNR values simulated with Matlab and measured by SRT of the following debris (ordered by RCS): VESSELSAT 2, COSMOS 1375, HJ-1A (first and second passage), CARTOSAT 2A, COSMOS 1408, COSMOS 2237 (first and second passage).

These reasons can be summarized in:

1) ***Transmitter power fluctuation***.

   As already said, the information about the transmitter were rather rough. So the authors of these work made some hypothesis in order to perform the simulations. Nevertheless one of the fundamental points in the analysis was the transmission power of 4 kW. But, according with others research groups (which have already worked with the FTS as a transmitter), there is a not negligible suspect that the transmitter power could suffer from some fluctuations in time. To prove this suspect some evaluations have been made. Since the acquisition chain of the SRT had never change during the campaign (except for VESSELSAT 2 which has not been included in this evaluation) the difference between the power received at the top of the chain and the power received at the bottom (named Pdiff) should have been the same for every debris. These differences have been estimate for some debris (sadly not for the entire list, because of the overlap of some debris power peak with the carrier), as can be seen in Table VII.

TABLE VII – Evaluated Pdiff.

Debris	Pdiff [dB]
COSMOS 2237 (second passage)	48.07
HJ-1A (first passage)	60.19
HJ-1A (second passage)	48.19
CARTOSAT 2A	42.16
COSMOS 1375	50.52

   Obviously the Pdiff is not always the same for every debris, so this support the hypothesis of transmission power fluctuation.

2) ***Peripheral passage of the debris inside the BIRALET beam***.

   Another point to take into account is that the previous evaluations have taken for granted the passage of the debris exactly in the center of the area illuminated by the BIRALET. This could not be true and if the debris was actually crossing a peripheral region of the beam the real SNR value would have been lesser than the simulated one by a maximum value of about 3 dB.

3) ***Inaccuracy of radar aiming***.

   This point is strictly related to the previous one. In order to obtain the azimuth and elevation pointing coordinates, during the 2014 campaign, the WXtrack software was used. Unfortunately the precision of WXtrack reaches only the first decimal place while the Python script used in this work can count in a

more precise value. So, if the aiming is not totally reliable the debris could not cross the center of the beam resulting in a decrease of the SNR value.

4) ***Mean RCS.***

The Radar Cross Section given by the Italian Air Force is probably the mean RCS for every debris. In this case if the debris is a flat objet the RCS may change depending on the debris orientation leading to a further inaccuracy in SNR evaluation.

5) ***Polarization.***

The FTS is capable of transmit signal in different polarization: RHCP, LHCP, VP, HP. This signal, depending on the type and shape of the debris, may change the polarization of the signal and arrive to the receiver with a different polarization. This aspect must be considered in the evaluation of the SNR.

Every one of these points could easily lead to an overestimation of the Signal-to-Noise Ratio in the simulation phase.

12. BIBLIOGRAPHY

[1] G. Pupillo. E. Salerno, M. Bartolini, M. Di Martino, A. Mattana, S. Montebugnoli, C. Portelli, S. Pluchino, F. Schillirò, A. Konovalenko, A. Nabatov, M. Nechaeva, "*The INAF contribution to the ASI Space Debris program: observational activities*", Mem. S.A.It. Suppl. Vol. 20, pp. 43-49, 2012.

[2] H. Klinkrad, T. Flohrer, H. Krag, K. Merz, "*Space operations – ESA and Space Debris*", European Space Agency, pp. 3-14, March 2013.

[3] "*Technical Report on Space Debris*", United Nations, New York, 1999.

[4] A. Morselli, P. Di Lizia, G. Bianchi, C. Bortolotti, S. Montebugnoli, G. Naldi, F. Perini, G. Pupillo, M. Roma, M. Schiaffino, A. Mattana, E. Salerno, A. Magro, K. Z. Adami, R. Armellin, A. L. Sergiusti, W. Villadei, F. Dolce, M. Reali, J. Paoli, "*A New High Sensitivity Radar Sensor for Space Debris Detection and Accurate Orbit Determination*", MetroAeroSpace, pp. 562-567, 2015.

[5] A. Morselli, R. Armellin, , P. Di Lizia, B. Zazzera, E. Salerno, G. Bianchi, S. Montebugnoli, A. Magro, K. Z. Adami, "*Orbit Determination of Space Debris Using a Bi-static Radar Configuration with a Multiple-Beam Receiver*", IAC-14-A6.9.4, pp. 1-11, 2014.

[6] P. Bolli, A. Orlati, L. Stringhetti, A. Orfei, S. Righini, R. Ambrosini, M. Bartolini, C. Bortolotti, F. Buffa, M. Buttu, A. Cattani, N. D'Amico, G. Deiana, A. Fara, F. Fiocchi, F. Gaudiomonte, A. Maccaferri, S. Mariotti, P. Marongiu, A. Melis, C. Migoni, M. Morsiani, M. Nanni, F. Nasyr, A. Pellizzoni, T. Pisanu, M. Poloni, S. Poppi, I. Porceddu, I. Prandoni, J. Roda, M. Roma, A. Scalambra, G. Serra, A. Trois, G. Valente, G. P. Vargiu, G. Zacchiroli, "*Sardinia Radio Telescope: General Description, Technical Commissioning and First Light*", Journal of Astronomical Instrumentation Vol. 4, nos. 4-5, 1550008 pp. 1-20, 2015.

[7] A. Morselli, R. Armellin, P. Di Lizia, F. Zazzera, E. Salerno, G. Bianchi, S. Montebugnoli, A. Magro, K. Adami, "*Orbit Determination of Space Debris Using a Bistatic Radar Configuration with a Multiple-Beam Receiver*", International Astronautical Congress A6.9.4, pp. 1-11, 2014.